Research Square

Preprints are preliminary reports that have not undergone peer review.
They should not be considered conclusive, used to inform clinical practice,
or referenced by the media as validated information.

Transcriptional benchmarking of human monocyte-derived microglia-like cells and iPSC-derived microglia reveals distinct immune-alert and homeostatic programmes

Hazel Quek

hazel.quek@qimrb.edu.au

QIMR Berghofer Medical Research Institute

Fazeleh Etebar

QIMR Berghofer Medical Research Institute

Carla Cuní-López

QIMR Berghofer Medical Research Institute

Jamie R. Kutasovic

The University of Queensland

Romal Stewart

QIMR Berghofer Medical Research Institute

Yi Chieh Lim

Nanyang Technological University

Tara L. Roberts

Western Sydney University

Anthony R. White

QIMR Berghofer Medical Research Institute

Short Report

Keywords: iPSC-derived microglia, monocyte-derived microglia, transcriptional profiling, neuroinflammation, neurodegeneration, in vitro models

Posted Date: July 28th, 2026

DOI: https://doi.org/10.21203/rs.3.rs-10477073/v1

License: This work is licensed under a Creative Commons Attribution 4.0 International License.
Read Full License

Additional Declarations: No competing interests reported.

Abstract

Human microglia play central roles in brain homeostasis, immune surveillance and neurodegeneration, yet *in vitro* human microglial models differ widely in cellular origin and culture context, complicating interpretation and translational application. Here, we systematically compare transcriptional and functional states across primary monocytes, monocyte-derived macrophages (MDMa), two-dimensional (2D) and three-dimensional (3D) monocyte-derived microglia-like cells (MDMi) and induced pluripotent stem cell-derived microglia (iPSC-iMG). Using targeted NanoString profiling, we interrogated key microglial biology categories including homeostatic microglial identity, purinergic signalling, TGF-β signalling, interferon responses, complement activation, antigen processing and presentation, phagocytosis and neurodegeneration-associated microglial neurodegenerative phenotype (MGnD)/ disease-associated microglia (DAM) programmes.

We find that cellular origin is a dominant determinant of microglial transcriptional identity. iPSC-iMG preferentially express homeostatic and CNS-patterned genes (*P2RY12*, *CX3CR1*, *ADORA1*) and TGF-β-associated regulators (*SMAD3*), consistent with a homeostatic microglial state. In contrast, MDMi retain immune-alert programmes characterised by interferon, complement and phagocytic gene modules (*IFIT1*, *STAT1*, *C1QA, C1QC*, *TREM2*, *APOE*), with partial overlap with MGnD/DAM-associated signatures. Despite these transcriptional differences, both models display comparable phagocytic uptake, indicating that distinct gene networks can support shared core functions.

Compared with 2D MDMi, 3D differentiation shifted toward a less immune-alert and more tissue-adapted microglia-like transcriptional state, characterised by increased expression of selected microglial identity-associated genes (*AIF1* and *TMEM119*) and reduced inflammatory and antigen-processing signatures (*IL18* and *CD74)*. However, 3D MDMi remained distinct from iPSC-iMG. Together, these data define model-specific baseline microglial states and provide a practical framework for selecting human microglial platforms for disease modelling and translational drug testing.

Introduction

Human microglia are central regulators of brain homeostasis, immune surveillance and neurodegeneration, yet modelling their biology *in vitro* remains an unresolved challenge. Advances in stem cell technologies and peripheral immune cell reprogramming have yielded multiple human microglial platforms, most notably induced pluripotent stem cell-derived microglia (iPSC-iMG) and monocyte-derived microglia-like cells (MDMi). These systems are now widely used to study neuroinflammation, genetic risk and therapeutic responses [1–3]. However, despite their increasing adoption, a fundamental question remains insufficiently addressed: to what extent do these models represent distinct microglial states at the transcriptional level?

Most comparative studies focus on selected microglial markers or functional assays, often treating different platforms as broadly interchangeable. This assumption is increasingly problematic. Microglia originate from embryonic yolk-sac progenitors and are shaped by the three-dimensional (3D)

architecture and signalling milieu of the central nervous system [4]. In contrast, MDMi are derived from adult peripheral monocytes and differentiated *in vitro*, typically under two-dimensional (2D) conditions [1, 5, 6]. While both systems express canonical microglial markers, the relative contributions of cellular origin and culture context to microglial transcriptional identity remain incompletely defined.

Increasing culture complexity through 3D matrices, neural-glial co-cultures and microglia-containing organoids has emerged as a strategy to better recapitulate the CNS microenvironment and promote microglial maturation [7–11]. These systems support CNS-relevant features, including ramified morphology, engagement of homeostatic and sensome pathways, phagocytosis, synaptic pruning and inflammatory responses [12–14]. However, it remains unclear how far increased culture complexity can shift monocyte-derived microglia-like cells/MDMi toward a CNS-like, homeostatic microglial state; or whether intrinsic peripheral lineage memory continues to shape their transcriptional and immune programmes [15, 16]. Direct transcriptional comparisons between 2D- and 3D-differentiated MDMi, and between MDMi and iPSC-derived microglia-like cells (iPSC-iMG) remain limited. Although iPSC-iMG are often positioned as the closest *in vitro* approximation to resident human microglia [2, 17], their relationship to peripheral immune programmes and disease-associated microglial states has not been systematically benchmarked against MDMi at pathway-level resolution.

Here, we address these gaps by performing targeted transcriptional profiling across human monocytes, monocyte-derived macrophages, 2D MDMi, 3D MDMi and iPSC-derived microglia using a curated glial gene panel. We first define baseline transcriptional differences between iPSC-derived and monocyte-derived microglial models and then assess how 3D differentiation reshapes monocyte-derived microglia/MDMi relative to monocytes and monocyte-derived macrophages. By comparing immune signalling, interferon responses, antigen processing, phagocytosis and neurodegeneration-associated microglial programmes, we show that cellular origin and culture dimensionality impose distinct constraints on microglial identity. These findings provide a practical framework for selecting human microglial models according to biological context, with implications for disease modelling and translational studies.

Results

Global transcriptional profiling distinguishes 2D and 3D MDMi from iPSC-iMG and other primary myeloid models

To directly compare 2D and 3D MDMi with iPSC-iMG, we profiled primary monocytes, MDMa, 2D MDMi, 3D MDMi and iPSC-iMG using the NanoString nCounter® Human Glial Profiling Panel (Fig. 1a). Phase-contrast imaging showed distinct morphologies across models and immunofluorescence confirmed IBA1-positive microglia-like phenotypes in 2D MDMi, 3D MDMi and iPSC-iMG, while MDMa were CD45-positive (Fig. 1b). Unsupervised hierarchical clustering separated monocyte progenitors from the differentiated myeloid models, with samples from the same cell type clustering together (Fig. 1c). For the primary-cell models, n = 2 independent biological donors were analysed, while the iPSC-iMG samples

comprised technical replicates from a single commercial Axol cell line and lot. Pearson correlation analysis showed a similar pattern, with samples grouping by cell type rather than donor (Fig. 1d). Principal component analysis (PCA) further indicated that cell type accounted for most transcriptional variation despite inter-donor differences (Fig. 1e).

Microglia-related genes showed clear model-dependent segregation (Fig. 1f). *AIF1 (*which encodes IBA1) was enriched across microglia-like conditions relative to monocytes and MDMa, while homeostatic markers, including *P2RY12*, *OLFML3*, *SALL1* were highest in iPSC-iMG, consistent with acquisition of a CNS-patterned, TGF-β-dependent microglial identity [2, 18]. *GAS6* was preferentially expressed across microglia-like models, including 2D MDMi, 3D MDMi and iPSC-iMG compared to monocytes and MDMa, while TGFBR1 remained broadly expressed, supporting a conserved role in homeostatic maintenance. In contrast, macrophage-associated genes (*USP2, SLC2A5 and ACAT2*) were selectively enriched in MDMa (Fig. 1g), while monocyte-associated genes (*FLT1, CCR5 and POR*) were highest in monocytes and reduced following differentiation (Fig. 1h). *CSF1R* remained expressed across differentiated models.

Immune activation genes indicated a stronger inflammatory signature in 2D MDMi compared with iPSC-iMG. *CCL2* was highly expressed in both 2D and 3D MDMi but remained low in iPSC-iMG, consistent with retention of peripheral chemokine programmes in monocyte-derived systems and their reduction as cells acquire a microglial identity [2, 18]. Interferon-responsive genes (*IFIT1, IFIT3*) and *IL18* were similarly elevated in 2D MDMi relative to iPSC-iMG, supporting a more pronounced immune-alert transcriptional state (Fig. 1i).

Relative to 2D MDMi and iPSC-iMG, 3D MDMi showed increased expression of tissue-adaptive and stress-associated genes (*SERPINA3* and *NPAS2)* (Fig. 1j). These findings indicate that 3D MDMi remain transcriptionally distinct from iPSC-iMG rather than uniformly converging towards the iPSC-derived state. Because the 3D MDMi platform also differed in culture duration and matrix context, these comparisons reflect differences between the complete culture systems rather than the isolated effect of dimensionality alone. Overall, these findings highlight clear transcriptional differences between monocyte, macrophage and microglia-like platforms, with cell type and differentiation state, rather than donor origin, driving major variation across human myeloid and MDMi models.

Direct comparison of 2D MDMi and iPSC-derived microglia reveals distinct model-specific states

Because 3D MDMi differ from iPSC-iMG in matrix context and culture duration, direct comparison was restricted to monocytes, 2D MDMi and iPSC-iMG. Monocytes were included as the progenitor reference.

To examine lineage-specific programmes, we examined curated microglial gene signatures representing “TGF-β Signalling”, “Homeostatic Microglia”, “Purinergic Signalling” and “Additional microglial markers” (canonical) (Fig. 2a). Both 2D MDMi and iPSC-iMG showed increased expression of canonical microglial-associated genes, including *C1QA* and *C1QB*, relative to monocytes, supporting acquisition of a shared

microglia-like identity. However, the two models differed across several homeostatic and signalling programmes, showing that both models share some microglial features but remain transcriptionally distinct.

Differential-expression analysis further confirmed these differences (Fig. 2b). Monocytes retained inflammatory and chemokine-associated genes, including *TNF*, *TGFB1*, *CCL3*, *CCR5*, FOS and *S100A12*, consistent with a peripheral immune profile. In contrast, 2D MDMi and iPSC-iMG showed increased expression of complement components (*C1QA*, *C1QB*, *C1QC*) and lysosomal/proteolytic genes (*CTSB*, *CTSD*, *LGMN*), supporting acquisition of surveillance and phagocytic-associated programmes. iPSC-iMG showed higher expression of genes associated with neuroimmune and receptor-mediated signalling (*GAD1*, *BDNF*, *FCGRT*, *ADRB1*, *HMGB1* and *GRM2*). By contrast, 2D MDMi preferentially expressed interferon-responsive genes including, *IFIT1*, *IFIT3* and *STAT1*, consistent with a more pronounced immune-alert state. Together, these data show that both 2D MDMi and iPSC-iMG shifted away from the monocyte transcriptional programme but adopted overlapping yet distinct microglia-like identities.

GO biological-process enrichment analysis supported these model-specific differences (Fig. 2c, d). Relative to monocytes, 2D MDMi were enriched for leukocyte migration, MAPK and ERK1/2 signalling, and broader immune and inflammatory processes. iPSC-iMG similarly showed enrichment of ERK/MAPK signalling and leukocyte chemotaxis pathways, indicating that both models engage immune-regulatory and signalling networks distinct from circulating monocytes. Functional assessment of phagocytic competence demonstrated progressive uptake over a 12 h time course in both 2D MDMi and iPSC-iMG (Fig. 2e; **Supplementary Fig. S3)**. Phagocytic area increased rapidly during the first 4–6 h before approaching a plateau in both models. Overall uptake were comparable between the two models indicating comparable functional clearance capacity. Phagocytosis-associated gene expression differed between models *C1QA*, *CTSB*, *LGMN*, *STAT1*, LILRB4 and *HLA-DR* were higher in 2D MDMi, while *ADORA1* and *DAP12* were higher in iPSC-iMG (Fig. 2f). These findings show that both models are phagocytically competent while retaining distinct transcriptional profiles.

Distinct immune and phagocytic programmes distinguish monocytes, MDMi and iPSC-iMG

To compare immune-related transcriptional programmes across human microglial models, we examined curated gene sets associated with phagocytosis, antigen processing and presentation, interferon signalling and complement pathways (Fig. 3a; **Supplementary Table S5)**.

Phagocytosis-related genes differed across the models. Monocytes expressed genes associated with peripheral phagocyte activity, including *BIN1* and *SPHK1*, while iPSC-iMG showed higher expression of *PAK1*, which regulates cytoskeletal remodelling during phagocytosis (Fig. 3b). Antigen-processing genes, including *TAP1* and *PSMC6*, were highest in monocytes and lower in both differentiated models. Interferon-associated genes also differed, with *IFIT3* highest in 2D MDMi, *TRIM2* higher in iPSC-iMG and

CD44 highest in monocytes. Complement genes, including *C1QA, C1QB, C1QC*, were more strongly expressed in the microglia-like models than in monocytes **(**Fig. 2f **and** Fig. 3a**)**.

We next compared the models against published MGnD, DAM stage 1 and DAM stage 2 reference signatures as defined in prior studies [19, 20] **(**Fig. 3c**)**. Both 2D MDMi and iPSC-iMG expressed selected MGnD/DAM-associated genes, including *TREM2*, *CTSD* and *APOE*, supporting development of lipid-sensing, lysosomal and phagocytic-remodelling programmes **(**Fig. 3d**)**. However, iPSC-iMG showed stronger expression of homeostatic microglial markers, including *P2RY12* and *CX3CR1*, while 2D MDMi retained a more inflammatory and antigen-presenting profile. *LPL* remained highest in monocytes, indicating that neither differentiated model uniformly reproduced the complete DAM or MGnD programme.

Notably, these MGnD/DAM signatures were used as reference points to compare gene expression, not to define disease states. Overall, 2D MDMi display stronger inflammatory, interferon and antigen-presentation features, while iPSC-iMG retain a more homeostatic microglial profile **(Supplementary Table S2)**. These findings highlight intrinsic, model-specific differences in immune and phagocytic programming across human microglial models at the transcriptomic level.

Three-dimensional culture selectively remodels the MDMi transcriptional state

To determine how culture architecture shapes MDMi identity, we compared primary monocytes, MDMa, 2D MDMi and Matrigel-embedded 3D MDMi. Curated gene signatures associated with purinergic signalling, homeostatic microglia, TGF-β signalling and additional microglial markers distinguished the four myeloid states (Fig. 4a). Both 2D and 3D MDMi expressed broader microglia-associated programmes than monocytes and MDMa, but 3D culture produced a selective rather than uniform shift in microglial gene expression.

To validate these transcriptomic patterns, targeted qRT–PCR was performed on selected representative genes **(**Fig. 4b**)**. Macrophage-associated markers, including *CD68*, *SLC2A5*, and *HAMP* were highest in MDMa. The microglial genes *AIF1* and *TMEM119* were most strongly expressed in 3D MDMi, while *P2RY12* was significantly higher in 2D MDMi. *GPR34* did not differ significantly between the two MDMi conditions. The lysosomal gene *LGMN* showed intermediate expression in MDMa and higher in MDMi systems, consistent with broader endolysosomal remodelling during myeloid differentiation.

GO enrichment further distinguished the differentiated states **(**Fig. 4c**)**. Relative to monocytes, MDMa were enriched for lipid metabolism, fatty-acid oxidation and related catabolic pathways. In contrast with MDMa, MDMi showed enrichment of defence response, vesicle-mediated transport, phagocytosis, leukocyte migration and inflammatory signalling pathways, supporting acquisition of immune surveillance and microglia-associated functional programmes. To capture coordinated pathway activity, we calculated module scores for key microglial and immune signatures **(**Fig. 4d**)**. Complement and

homeostatic microglial scores were higher in both MDMi models, while antigen-presentation activity was strongest in MDMa. Interferon, inflammasome and phagocytosis-related scores varied across the models, further supporting distinct rather than progressively ordered myeloid states.

Overall, MDMi systems showed a stepwise transition from circulating monocytes toward microglia-like states, with 3D MDMi showing the strongest alignment with homeostatic microglial gene programmes. In contrast, MDMa retained lipid-metabolic and inflammatory features characteristic of peripheral myeloid cells.

Discussion

Human microglia models are increasingly used to interrogate neuroinflammation, genetic risk and therapeutic response, yet there remains no clear framework for defining which microglial states are captured by different *in vitro* platforms. This remains a major challenge because microglial identity is heterogeneous and shaped by both ontogeny and local environmental cues [21–23]. Loss of the CNS niche can therefore substantially alter microglial transcriptional state [12, 15, 18, 24, 25]. Here, using targeted transcriptional profiling across monocytes, MDMa, 2D MDMi, 3D MDMi and iPSC-iMG, we show that cellular origin and culture conditions shape microglial identity.

This comparative analysis highlights three key features of human microglial model identity. First, iPSC-iMG showed a strong bias toward a homeostatic, CNS-patterned microglia-like programme, marked by higher expression of *P2RY12*, *CX3CR1* and TGF-β-linked modules. This is consistent with studies showing that iPSC-derived microglia-like cells can acquire key microglial identity markers and functional phagocytic capacity [26, 27]. Thus, iPSC-iMG provide a useful reference for core features of resident microglial identity, while their transcriptional state remains shaped by the maturation cues and environmental context available within the *in vitro* system. This homeostatic bias is relevant for studies of microglial surveillance, lipid handling, lysosomal function and TREM2/APOE-associated pathways, but also highlights that iPSC-iMG and MDMi should be treated as complementary platforms [20, 28].

Second, MDMi acquired core microglia-like features, including complement, lysosomal and phagocytic programmes, but retained stronger immune-alert wiring than iPSC-iMG. This was most evident in 2D MDMi, which showed enrichment of interferon-responsive genes, antigen-processing machinery and inflammatory modules. These findings are consistent with prior work showing that monocytes can be differentiated into functionally competent microglia-like cells [1, 6, 12], while also supporting the view that peripheral ontogeny leaves a persistent transcriptional imprint. This immune-primed baseline may be advantageous for modelling inflammatory effector functions, complement-linked responses and phagocytic remodelling, but it should be considered when using MDMi to study homeostatic or synapse-supportive microglial functions. The partial alignment of MDMi with DAM/MGnD-associated signatures further supports this interpretation.

The overlap between MDMi and published DAM/MGnD signatures was selective rather than uniform. Importantly, several genes commonly associated with DAM or MGnD states were not specific to MDMi.

APOE and *LPL* were strongly expressed in MDMa, while TREM2 was highest in 3D MDMi and MDMa. These patterns indicate that such genes can reflect broader myeloid lipid-sensing, lysosomal and phagocytic programmes rather than a disease-associated microglial state specifically. The apparent MDMi overlap was instead driven by selected combinations of complement, lysosomal and immune-remodelling genes, including *C1QA*, *C1QB*, *C1QC*, *CTSD*, *GPNMB*, *AXL* and *LYZ*. Accordingly, gene-set enrichment should be interpreted alongside the expression of the individual genes contributing to each module, as a module score may be driven by a subset of highly expressed genes rather than coordinated activation of the complete reference programme. Our findings therefore do not indicate that baseline MDMi represent DAM or MGnD cells, but that they share selected transcriptional features with these states.

A key implication of these findings is that similar functional outcomes can be supported by different transcriptional programmes. In this study, 2D MDMi and iPSC-iMG showed progressive phagocytic uptake under the conditions tested, despite clear differences in phagocytosis-associated gene expression. These similar uptake profiles do not necessarily reflect equivalent molecular regulation. It is also possible that some genes assigned to phagocytosis-related modules primarily reflect broader lysosomal, inflammatory or cytoskeletal states rather than directly controlling uptake in this assay. Moreover, transcript abundance does not establish corresponding protein abundance, localisation or pathway activity. Protein-level and mechanistic studies will therefore be required to determine which pathways directly support phagocytosis in each model. This distinction is important for therapeutic screening, as compounds that modify phagocytosis, lysosomal activity or inflammation in one platform may have different effects in another if the regulatory programmes differ [7, 10, 29–32]. Human microglial transcriptomic studies also support this context dependence, showing that inflammatory, interferon and antigen-processing programmes vary across brain region, pathology and different functional microglial states [33–35].

Finally, we asked whether 3D culture can shift MDMi toward a more CNS-like state. Relative to 2D MDMi, 3D MDMi showed increased expression of the microglia-associated genes, including *TMEM119* and *AIF1*, together with lower expression of selected inflammatory and antigen-processing genes including *IL18*, *LILRB4*, *HLA-A* and *P2RX7* (**Supplementary Table S2**). This is consistent with studies showing that environmental cues are critical for establishing and maintaining microglial identity [12, 15, 36], and with studies showing that matrix-supported 3D culture environments, organoids and co-culture systems can modulate inflammatory responses and promote aspects of microglial identity, morphology and maturation *in vitro* [7, 8, 37, 38].

The inclusion of MDMa provided an additional reference point for distinguishing microglia-like differentiation from broader macrophage differentiation. MDMa retained stronger lipid-metabolic and inflammatory features, consistent with a peripheral macrophage-like state, while MDMi showed greater enrichment of microglial identity, purinergic, complement and phagocytic programmes. This comparison supports the interpretation that MDMi are transcriptionally distinguishable from conventionally differentiated MDMa, while still retaining features of peripheral myeloid origin.

Overall, 3D differentiation attenuated features of the 2D immune-alert state but did not fully erase monocyte lineage influence or drive convergence with iPSC-iMG. These findings are consistent with recent work by Li *et al*., who showed that human iPSC-derived neuron-astrocyte-microglia tri-cultures substantially remodel microglial transcriptional states, including programs associated with endocytosis, neuron-related functions, ferroptosis, stress response and autophagy [39]. Together, these data suggest that microglia-like maturation is not governed by dimensionality alone but is shaped by the combined effects of extracellular matrix composition, cytokine context, culture duration and the presence of neuronal, astrocytic or other CNS-associated cues. These findings position MDMi as a useful human platform for studying donor-specific microglial-like immune function, while highlighting that MDMi are complementary rather than interchangeable with iPSC-iMG or resident brain microglia.

Limitations of the study

This study uses a curated ~ 770-gene panel, which enables robust, interpretable pathway comparisons but cannot fully capture transcriptome-wide programmes or cell-state heterogeneity at single-cell resolution. The analysis was also limited to RNA abundance and therefore did not assess post-transcriptional regulation, protein expression, protein localisation or pathway activity, all of which may substantially influence microglial function. Replicate structure also differed across platforms (iPSC-iMG were represented by technical replicates from one line, while primary-cell-derived models were represented by biological replicates from independent donors) and culture durations were not identical across conditions. These factors may influence specific modules, particularly stress and maturation-linked pathways. Future studies using larger donor cohorts, multiple iPSC lines and matched culture durations will be needed to define how stable these platform-specific states are across genetic backgrounds and experimental contexts.

Materials and Methods

Culture of commercially sourced human iPSC-derived microglia

Cryopreserved human iPSC-derived mature microglia (iPSC-iMG) were obtained from Axol Bioscience (Cat. No. ax0668, Lot No. 0668091219, female donor, newborn; no reported disease). Cells were generated from cord blood-derived $CD34^+$ cells using an episomal reprogramming approach and differentiated in fully defined medium through an intermediate monocyte stage prior to terminal microglial specification. Cells were supplied cryopreserved as adherent, terminally differentiated microglia. Cells were stored in vapour-phase liquid nitrogen and shipped on dry ice prior to use. For culture, cells were maintained in Microglia Maintenance Medium (Cat. No. ax0660; Axol Bioscience), a proprietary formulation optimised for mature microglial stability.

Prior to cell seeding, culture vessels were coated with Matrigel (Corning) following the manufacturer's instructions to promote cell attachment. Cells were rapidly thawed and resuspended in Microglia

Maintenance Medium supplemented with RevitaCell (Thermo Fisher Scientific; 1:100 dilution) to enhance post-thaw viability, then plated at 1×10^5-$3x10^5$ cells/cm^2. After 24 h, a complete medium change was performed using fresh Microglia Maintenance Medium without RevitaCell. Thereafter, half-medium changes were performed every other day. Cells were maintained in culture for 14 days post-thaw prior to experimental use to allow stabilisation and maturation *in vitro*. Microglial identity was confirmed by positive immunostaining for Iba1 (019-19741; 1:500; Wako) and functional competence was assessed using a phagocytosis assay.

Generation of monocyte-derived microglia-like cells (MDMi)

Human MDMi were generated from peripheral blood mononuclear cells as previously described [40]. PBMCs were isolated from whole blood obtained from healthy donors by density-gradient centrifugation using Lymphoprep (STEMCELL Technologies) and plated onto Matrigel-coated plates (Corning) at a seeding density of 4–5 × 10^5 cells/cm^2. Cells were cultured in RPMI-1640 medium supplemented with 10 ng/mL GM-CSF and 100 ng/mL IL-34 (both from Thermo Fisher Scientific) and maintained under 2D or 3D conditions. For 3D cultures, cells were embedded within a Matrigel matrix to provide spatial context, as described [7]. Culture medium was replaced every 3 days for both 2D and 3D conditions. 2D MDMi were maintained for 14 days, while 3D MDMi were cultured for 30 days prior to downstream analyses.

Generation of monocyte-derived macrophages (MDMa)

Monocyte-derived macrophages (MDMa) were generated from PBMCs cultured in RPMI-1640 GlutaMAX™ supplemented with 10% heat-inactivated fetal bovine serum (FBS) and 10 ng/mL GM-CSF as previously described [5]. Cells were maintained for 14 days, with medium changes performed every 3 days. MDMa generated under these conditions exhibited characteristic macrophage morphology, including an enlarged cell surface area and an amoeboid morphology, which was clearly distinct from the ramified morphology observed in monocyte-derived microglia-like cells (MDMi).

RNA isolation and NanoString glial profiling panel

Targeted transcriptional profiling was performed using the NanoString nCounter® Human Glial Profiling Panel (~ 770 genes) across five human myeloid and microglial-like platforms: monocytes, MDMa, 2D MDMi, 3D MDMi and iPSC-iMG. The primary-cell models were generated from two independent healthy male blood donors, both < 40 years of age, using a donor-matched experimental design. Mono1, MDMa1, MDMi1 and 3D_MDMi1 were generated from donor 1, while Mono2, MDMa2, MDMi2 and 3D_MDMi2 were generated from donor 2. Thus, each donor contributed all four primary-cell conditions, permitting within-donor comparison across monocytes, MDMa, 2D MDMi and 3D MDMi. iPSC-iMG samples were obtained from a single commercially sourced Axol cell line and lot (Cat. No. ax0668; Lot No. 0668091219). The line was generated by episomal reprogramming of cord blood-derived $CD34^+$ cells obtained from a female donor sampled at birth, with no reported disease.

Total RNA was extracted using TRIzol™ Reagent (Thermo Fisher) according to the manufacturer's instructions. The panel comprised 757 glial- and neurobiology-related target genes and 13 internal reference (housekeeping) genes, spanning pathways associated with microglial identity and activation, immune signalling, cellular stress responses, neuroinflammation and neurotransmission (**Supplementary Fig. S1**).

Hybridisation reactions were performed using the NanoString nCounter Human Glial Profiling Panel according to the manufacturer's instructions (MAN-10056-05). Briefly, 120 ng total RNA in a final volume of 5 µL was hybridised with barcoded reporter probes and biotinylated capture probes at 65°C for 18 h. Probe handling was performed according to manufacturer guidelines to preserve probe integrity (no vortexing; gentle mixing by inversion and low-speed centrifugation ≤ 1,000 × g). Following hybridisation, samples were processed on the nCounter Prep Station (MAN-C0035-07), where excess probes were removed and target-probe complexes were purified using magnetic bead-based capture and immobilised in nCounter cartridges. Cartridges were then transferred to the nCounter Digital Analyzer for imaging and barcode counting, using maximum field-of-view (FOV) settings (555 FOV per sample) to maximise sensitivity. Raw barcode counts were extracted using nSolver software (NanoString Technologies).

Quality control was assessed using built-in positive and negative controls. Two biological donors were analysed for each primary-cell condition, comprising monocytes, MDMa, 2D MDMi and 3D MDMi. iPSC-iMG were represented by two technical replicates from one commercial cell line and lot. The complete list of genes, functional annotations and pathway classifications included in the Glial Profiling Panel is provided in **Supplementary Table S1**.

NanoString data processing and differential expression analysis

Raw NanoString counts were imported into nSolver Analysis Software v4.0 (NanoString Technologies) for quality control and normalisation (**Supplementary Fig. S2)**. Built-in positive and negative controls were assessed for quality control. Positive-control normalisation was performed using POS_A-POS_F and the geometric mean. CodeSet content normalisation was then performed using the geometric mean of ten reference genes selected for stable expression: *ASB7, CCDC127, CSNK2A2, FAM104A*, *LARS1, MTO1, SUPT7L, TADA2B, TBP and XPNPEP1*. The resulting normalised expression values were exported for downstream statistical analyses in R (v4.0.5)[41] and are provided in **Supplementary Table S2**.

For exploratory analysis, normalised expression values were $\log_2$-transformed where appropriate and subjected to principal component analysis (PCA) using the prcomp function on variance-scaled data. Principal component scores were visualised using the ggplot2 package, and the percentage of variance explained by each principal component was calculated from the PCA output and displayed on the corresponding axes. Differential expression analysis was performed using the limma package in R. Log_2-transformed normalised expression values were analysed using linear models with empirical Bayes moderation. For pairwise comparisons, contrasts were specified within the linear modelling framework. For reference-based analyses, monocytes were used as the baseline condition, and separate linear

models were fitted for each *in vitro* model (MDMi, iPSC-iMG, 3D MDMi and MDMa) relative to monocytes. *P*-values were adjusted for multiple testing using the Benjamini-Hochberg method to control the false discovery rate (FDR). Genes were considered differentially expressed when they met both $|\log_2$ fold change$|$ > 1 and FDR < 0.05 (**Supplementary Table S3**). Heatmaps were generated using the pheatmap package to visualise expression patterns of selected gene sets. Log_2-transformed expression values were standardised on a per-gene basis using row-wise z-score normalisation. For condition-level visualisation, biological replicates were averaged within each experimental group prior to scaling. Hierarchical clustering was performed using Euclidean distance and complete linkage unless otherwise specified. The raw and normalised NanoString expression data have been deposited in the NCBI Gene Expression Omnibus under accession number GSE339569.

Functional enrichment analysis

Functional enrichment analyses were performed using the clusterProfiler package. Gene symbols were converted to Entrez identifiers using org.Hs.eg.db. Gene Ontology (GO) enrichment analysis was conducted for Biological Process (BP). Enrichment significance was determined using Benjamini-Hochberg adjusted *p*-values. Results were visualised using dot plots.

Module scoring and comparison across myeloid differentiation conditions

To quantify coordinated transcriptional programmes, curated gene modules representing microglial homeostatic and activation-associated pathways were defined a priori. These included Homeostatic Microglia, Purinergic Signalling, TGF-β Signalling, Interferon Signalling, Antigen Presentation, Complement System, Inflammasome and Phagocytosis. For each module, only genes detected in the expression dataset were retained. Module scores were calculated using a gene-wise standardisation approach. Expression values were first standardised per gene across all samples using *z*-score transformation to ensure equal weighting of genes within each module. For each sample, module scores were defined as the mean *z*-scored expression of all genes belonging to that module, generating a matrix of samples × modules. Module scores were visualised as faceted boxplots to illustrate condition-specific transcriptional programmes and replicate-level variation.

Real-time qPCR

RNA extraction and cDNA synthesis were performed as previously described [5]. Briefly, total RNA was isolated using TRIzol™ reagent (Thermo Fisher Scientific, CA, USA) according to the manufacturer's instructions. Complementary DNA (cDNA) was generated using the SensiFAST™ cDNA Synthesis Kit (Bioline, London, UK). For quantitative real-time PCR (qRT-PCR), cDNA was diluted 1:10 and amplified using SensiFAST™ SYBR® Lo-ROX Master Mix with gene-specific primers. Reactions were run in technical triplicate on a QuantStudio™ 5 Real-Time PCR System (Thermo Fisher Scientific, CA, USA). Delta cycle threshold (ΔCT) values were normalised to 18S and used to determine relative gene expression between samples. Melting curve analyses confirmed a single melting peak for all primers.

Primer sequences for human genes are provided in **Supplementary Table S4**. Technical qRT-PCR wells were averaged before analysis and were not treated as independent observations.

Phagocytosis assay

Phagocytic activity was assessed in both 2D MDMi and iPSC-iMG using real-time live-cell imaging on the IncuCyte S3 system (Essen Bioscience). Cells were incubated with sonicated, fluorescent pHrodo™-labelled Escherichia coli bioparticles (Thermo Fisher Scientific, USA). Images were acquired hourly over a 12-h period at 10× magnification using phase-contrast and red fluorescence channels. Image acquisition and quantitative analysis were performed using IncuCyte analysis software (version 2024A). Background fluorescence was removed using a top-hat thresholding algorithm, with all analysis parameters held constant across experimental conditions and cell models. Phagocytic activity was calculated as the ratio of red fluorescent object area to phase-contrast object count at each time point.

Statistical analysis

Normality of qRT-PCR data was assessed using the Shapiro-Wilk test. Multiple-group comparisons were analysed using ordinary one-way ANOVA followed by Tukey's or Dunnett's multiple-comparisons test, as appropriate. Selected two-group comparisons were analysed using two-tailed Welch's *t*-tests. Analyses were performed using GraphPad Prism version 10.6.1 (GraphPad Software), with $P < 0.05$ considered statistically significant.

Declarations

Acknowledgements

We thank the volunteers from QIMRB-MRI who have donated blood to this project.

Funding

This research was funded by the National Health and Medical Research Council of Australia (NHMRC) (APP1125796), a National Foundation for Medical Research and Innovation (NFMRI) grant, and a US Dept Defense CDMRP ALS grant (W81XWH-22–1-0714) to ARW. ARW was supported by an NHMRC Senior Research Fellowship (APP1118452), and HQ was supported by an NHMRC Ideas grant (APP2029183) and MND Research Australia Fat Rabbit Innovator grant (IG_2439).

Competing Interests

The authors have no relevant financial or non-financial interests to disclose.

Author Contributions

Conceptualization: HQ, FE, ARW. Methodology: HQ, FE, CC-L, JRK, RS, YCL, TLR. Investigation: HQ, FE, CC-L. Visualization: HQ, FE. Funding acquisition: HQ, ARW. Project administration: ARW. Supervision:

ARW. Writing-review and editing: HQ, FE, CC-L, JRK, RS, YCL, TLR, ARW. All authors read and approved the final manuscript.

Data Availability

The NanoString dataset generated in this study is available in the NCBI Gene Expression Omnibus under accession number GSE339569. Additional data supporting the findings of this study are available from the corresponding author upon reasonable request.

Ethical Approval

All research adhered to the ethical guidelines on human research outlined by the National Health and Medical Research Council of Australia (NHMRC). Ethical approval was granted by the QIMR Berghofer Medical Research Institute Human Research Ethics Committee (P2197).

Consent to participate

Informed consent was obtained from all individual participants included in the study.

Consent for publication

Not applicable.

References

1. Ryan KJ et al (2017) A human microglia-like cellular model for assessing the effects of neurodegenerative disease gene variants. Sci Transl Med, 9(421)
2. Abud EM et al (2017) iPSC-Derived Human Microglia-like Cells to Study Neurological Diseases. Neuron 94(2):278–293e9
3. Summers RA et al (2024) Novel human iPSC models of neuroinflammation in neurodegenerative disease and regenerative medicine. Trends Immunol 45(10):799–813
4. Ginhoux F et al (2010) Fate mapping analysis reveals that adult microglia derive from primitive macrophages. Science 330(6005):841–845
5. Quek H et al (2022) ALS monocyte-derived microglia-like cells reveal cytoplasmic TDP-43 accumulation, DNA damage, and cell-specific impairment of phagocytosis associated with disease progression. J Neuroinflammation 19(1):58
6. Ohgidani M et al (2014) Direct induction of ramified microglia-like cells from human monocytes: dynamic microglial dysfunction in Nasu-Hakola disease. Sci Rep 4:4957
7. Cuní-López C et al (2024) Advanced patient-specific microglia cell models for pre-clinical studies in Alzheimer's disease. J Neuroinflammation 21(1):50
8. Rittenhouse A et al (2025) Microglia-containing neural organoids as brain microphysiological systems for long-term culture. Front Cell Neurosci, Volume 19–2025

9. Park DS et al (2023) iPS-cell-derived microglia promote brain organoid maturation via cholesterol transfer. Nature 623(7986):397–405
10. Han CZ et al (2023) Human microglia maturation is underpinned by specific gene regulatory networks. Immunity 56(9):2152–2171e13
11. Cuní-López C et al (2023) 3D in vitro modelling of human patient microglia: A focus on clinical translation and drug development in neurodegenerative diseases. J Neuroimmunol 375:578017
12. Etebar F, White AR, Quek H (2026) Microglial heterogeneity: influence of human 2D, 3D, and co-culture models on gene expression and immune function. Front Cell Neurosci 20:1770518
13. Xu R et al (2021) Developing human pluripotent stem cell-based cerebral organoids with a controllable microglia ratio for modeling brain development and pathology. Stem Cell Rep 16(8):1923–1937
14. Wenzel TJ, Desjarlais JD, Mousseau DD (2024) Human brain organoids containing microglia that have arisen innately adapt to a β-amyloid challenge better than those in which microglia are integrated by co-culture. Stem Cell Res Ther 15(1):258
15. Gosselin D et al (2017) An environment-dependent transcriptional network specifies human microglia identity. Science, 356(6344)
16. Cadiz MP et al (2022) Culture shock: microglial heterogeneity, activation, and disrupted single-cell microglial networks in vitro. Mol Neurodegener 17(1):26
17. Douvaras P et al (2017) Directed Differentiation of Human Pluripotent Stem Cells to Microglia. Stem Cell Rep 8(6):1516–1524
18. Bennett ML et al (2016) *New tools for studying microglia in the mouse and human CNS.* Proceedings of the National Academy of Sciences, 113(12): pp. E1738-E1746
19. Keren-Shaul H et al (2017) A Unique Microglia Type Associated with Restricting Development of Alzheimer's Disease. Cell 169(7):1276–1290e17
20. Krasemann S et al (2017) The TREM2-APOE Pathway Drives the Transcriptional Phenotype of Dysfunctional Microglia in Neurodegenerative Diseases. Immunity 47(3):566–581e9
21. Priller J, Prinz M (2019) Targeting microglia in brain disorders. Science 365(6448):32–33
22. Depp C et al (2025) Microglia transcriptional states and their functional significance: Context drives diversity. Immunity 58(5):1052–1067
23. Mancuso R et al (2024) Xenografted human microglia display diverse transcriptomic states in response to Alzheimer’s disease-related amyloid-β pathology. Nat Neurosci 27(5):886–900
24. Butovsky O et al (2014) Identification of a unique TGF-β-dependent molecular and functional signature in microglia. Nat Neurosci 17(1):131–143
25. Safaiyan S et al (2021) White matter aging drives microglial diversity. Neuron 109(7):1100–1117e10
26. Muffat J et al (2016) Efficient derivation of microglia-like cells from human pluripotent stem cells. Nat Med 22(11):1358–1367

27. Haenseler W et al (2017) A Highly Efficient Human Pluripotent Stem Cell Microglia Model Displays a Neuronal-Co-culture-Specific Expression Profile and Inflammatory Response. Stem Cell Rep 8(6):1727–1742
28. Ulland TK, Colonna M (2018) TREM2 - a key player in microglial biology and Alzheimer disease. Nat Rev Neurol 14(11):667–675
29. Sellgren CM et al (2019) Increased synapse elimination by microglia in schizophrenia patient-derived models of synaptic pruning. Nat Neurosci 22(3):374–385
30. Saeki K, Ozato K (2025) Transcription factors that define the epigenome structures and transcriptomes in microglia. Exp Hematol 149:104814
31. Troutman TD, Kofman E, Glass CK (2021) Exploiting dynamic enhancer landscapes to decode macrophage and microglia phenotypes in health and disease. Mol Cell 81(19):3888–3903
32. Cuní-López C et al (2025) Exploring a patient-specific in vitro pipeline for stratification and drug response prediction of microglia-based therapeutics. Sci Rep 15(1):8296
33. van der Poel M et al (2019) Transcriptional profiling of human microglia reveals grey–white matter heterogeneity and multiple sclerosis-associated changes. Nat Commun 10(1):1139
34. Olah M et al (2020) Single cell RNA sequencing of human microglia uncovers a subset associated with Alzheimer's disease. Nat Commun 11(1):6129
35. Mathys H et al (2019) Single-cell transcriptomic analysis of Alzheimer's disease. Nature 570(7761):332–337
36. Etebar F et al (2026) *Regional and sub-regional microglial heterogeneity in the steady-state mouse brain and retina.* bioRxiv, : p. 2026.01.16.699866
37. Wu J et al (2026) *Human microglia in brain assembloids display region-specific diversity and respond to hyperexcitable neurons carrying < i>SCN2A* mutation. Sci Adv 12(8):eady2977
38. Bohlen CJ et al (2017) Diverse Requirements for Microglial Survival, Specification, and Function Revealed by Defined-Medium Cultures. Neuron 94(4):759–773e8
39. Li HL et al (2026) Microglial dynamics and ferroptosis induction in human iPSC-derived neuron–astrocyte–microglia tri-cultures. FEBS Open Bio 16(6):1060–1073
40. Quek H et al (2022) A robust approach to differentiate human monocyte-derived microglia from peripheral blood mononuclear cells. STAR Protoc 3(4):101747
41. Team RC (2021) *R: A language and environment for statistical computing*, in *R Foundation for Statistical Computing, Vienna, Austria*

Figures

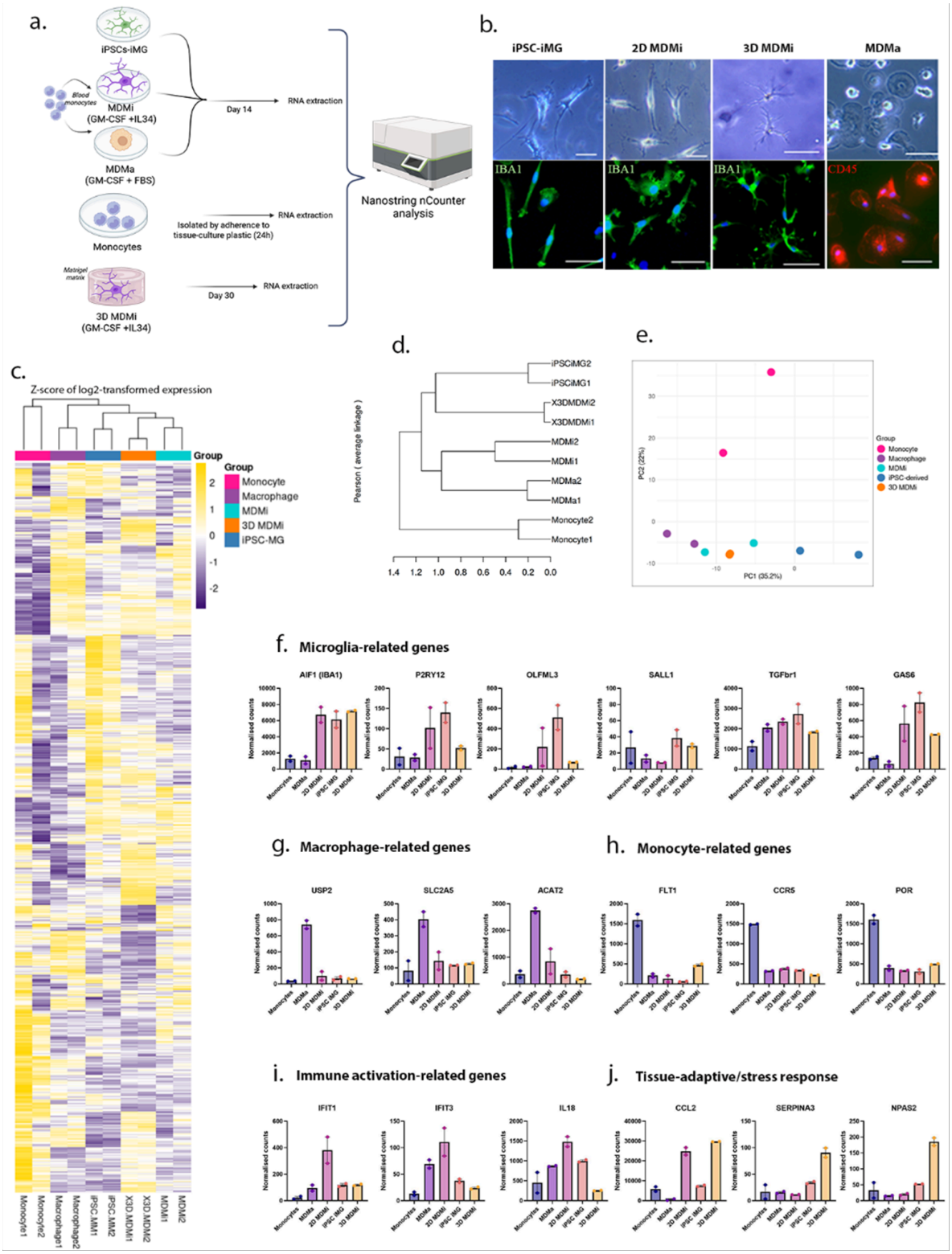


Figure 1

Transcriptional profiling in human myeloid and microglia-like models. (a) Schematic overview of model generation, including monocytes, MDMa, 2D and 3D MDMi and iPSC-iMG, followed by NanoString nCounter profiling of 770 myeloid and neuroinflammation-related genes. **(b)** Representative phase-contrast and immunofluorescence images showing distinct morphologies across models. iPSC-iMG, 2D MDMi and 3D MDMi were IBA1-positive, while MDMa are CD45-positive. **(c)** Heatmap of unsupervised

hierarchical clustering showing separation of monocyte progenitors from differentiated myeloid models, with replicates clustering by condition. **(d)** Pearson correlation clustering showing grouping by cell type rather than donor for primary-cell-derived models. **(e)** PCA showing separation along the major axis of myeloid differentiation. **(f-j)** Selected gene sets highlighting **(f)** microglial-related genes, **(g)** macrophage-related genes, **(h)** monocyte-related genes, **(i)** immune activation related, and **(j)** tissue-adaptive/stress responses. Bars show the mean, whiskers indicate the range and points represent individual measurements. Monocytes, MDMa, 2D MDMi and 3D MDMi were generated from two matched biological donors; iPSC-iMG samples represent technical replicates from one iPSC line. Scale bars, 50 µm

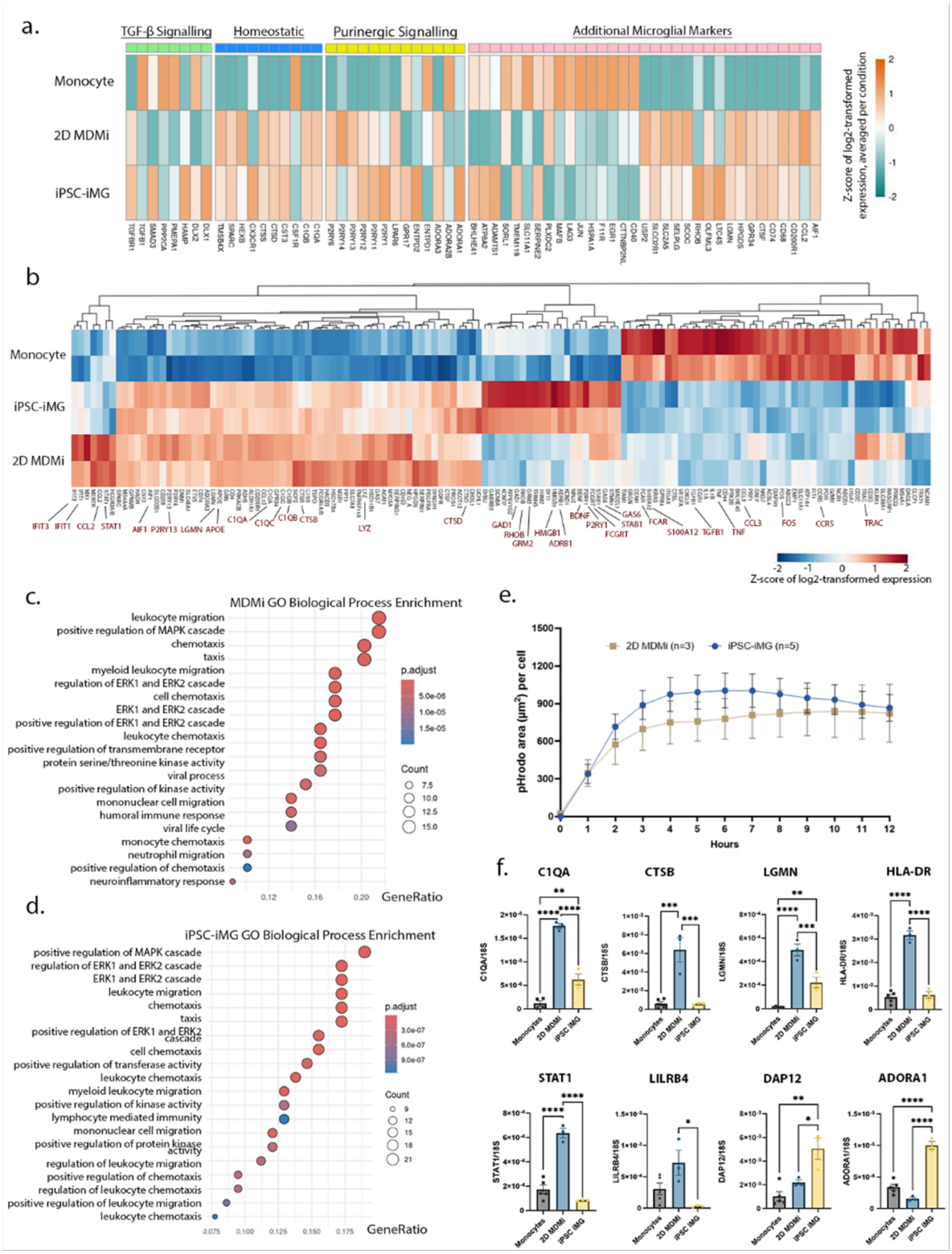


Figure 2

Distinct transcriptional and functional profiles of 2D MDMi and iPSC-iMG. (a) Heatmap of curated microglial gene signatures grouped into functional categories. Values represent *z*-scores of log2-transformed expression averaged per condition. **(b)** Unsupervised hierarchical clustering of differentially expressed genes across monocytes, 2D MDMi and iPSC-iMG. Selected genes highlighted in red indicate key genes distinguishing conditions. **(c-d)**GO biological process enrichment analysis of differentially

expressed genes in **(c)**2D MDMi and **(d)** iPSC-iMG relative to monocytes. Dot plots show enriched pathways, with gene ratio on the x-axis and adjusted *p*-value indicated by colour scale. **(e)** Live-cell phagocytosis kinetics measured over 12 h using pHrodo™-labelled *E. coli* bioparticles. 2D MDMi were derived from three independent biological donors, while iPSC-iMG measurements represent five technical wells from one commercial cell line. Data are shown as the mean ± SD. **(f)** qRT-PCR validation of phagocytosis-related gene expression markers across monocytes (n = 5 biological replicates), 2D MDMi (n = 3 biological replicates), and iPSC-iMG (n = 3 technical replicates). Individual values are shown; bars represent the mean and range. Statistical analyses were performed as described in Methods. $P < 0.05$ (*), $P < 0.01$ (**), $P < 0.001$ (***), $P < 0.0001$ (****)

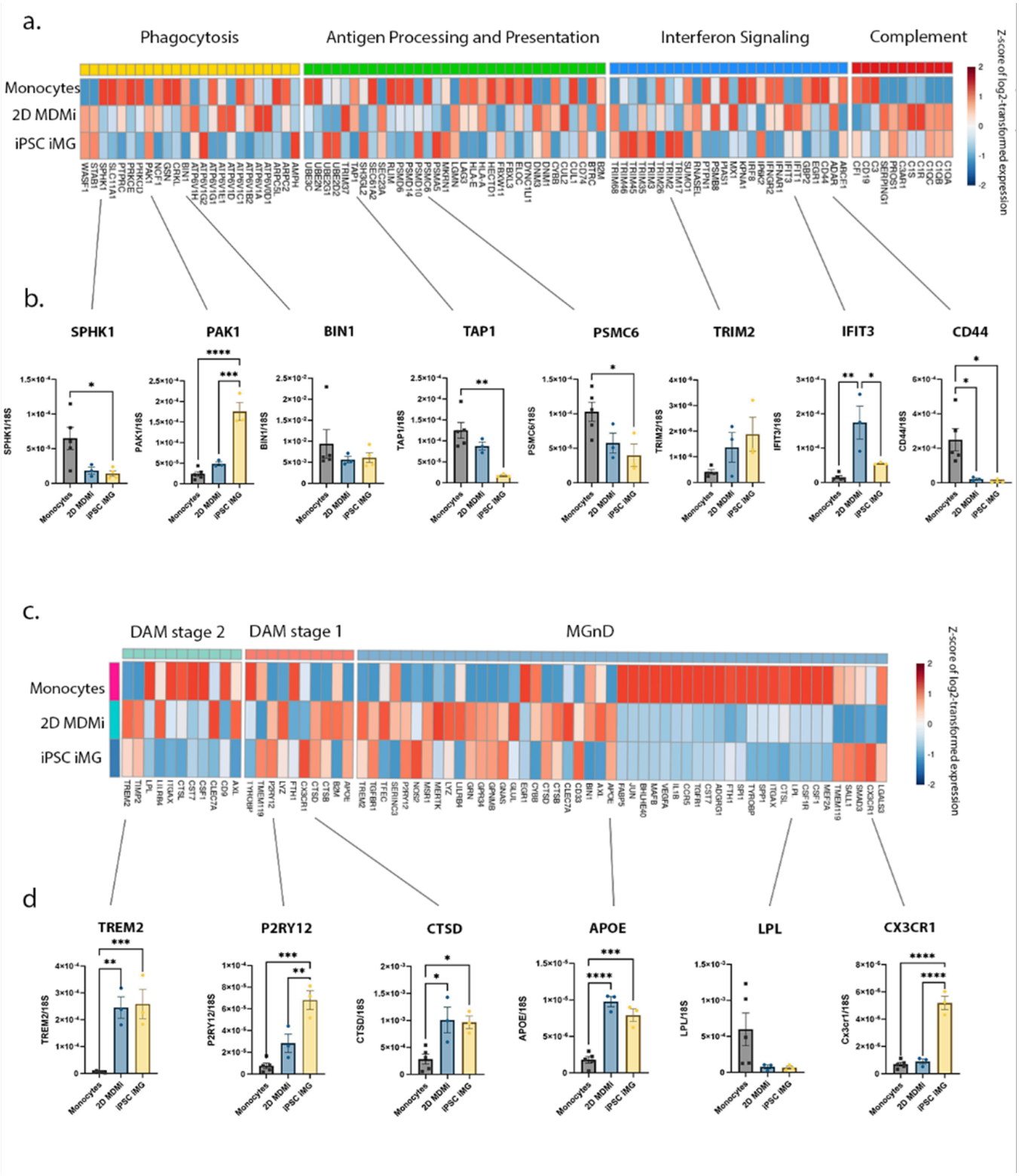


Figure 3

Differential immune and DAM/MGnD-associated gene signatures across monocytes, 2D MDMi and iPSC-iMG (a) Heatmap of curated immune pathway gene sets, including Phagocytosis, Antigen Processing and Presentation, Interferon Signalling and Complement pathways. Values represent *z*-scores of log2-transformed expression. **(b)** Targeted qRT–PCR validation of selected genes from Phagocytosis, Antigen Processing and Presentation, and Interferon signalling categories across

conditions. **(c)**Heatmap of DAM stage 1, DAM stage 2 and MGnD gene signatures across models. Values represent *z*-scores of log2-transformed expression. **(d)**Targeted qRT–PCR validation of selected DAM- and microglia-associated genes across conditions. For panels (b and d), monocytes represent n = 5 independent biological donors, 2D MDMi represent n = 3 independent biological donors and iPSC-iMG represent technical triplicates from one commercial cell line. Individual values are shown, with bars representing the mean and range. Statistical analyses were performed as described in the Methods. $P < 0.05$ (*), $P < 0.01$ (**), $P < 0.001$ (***), $P < 0.0001$ (****)

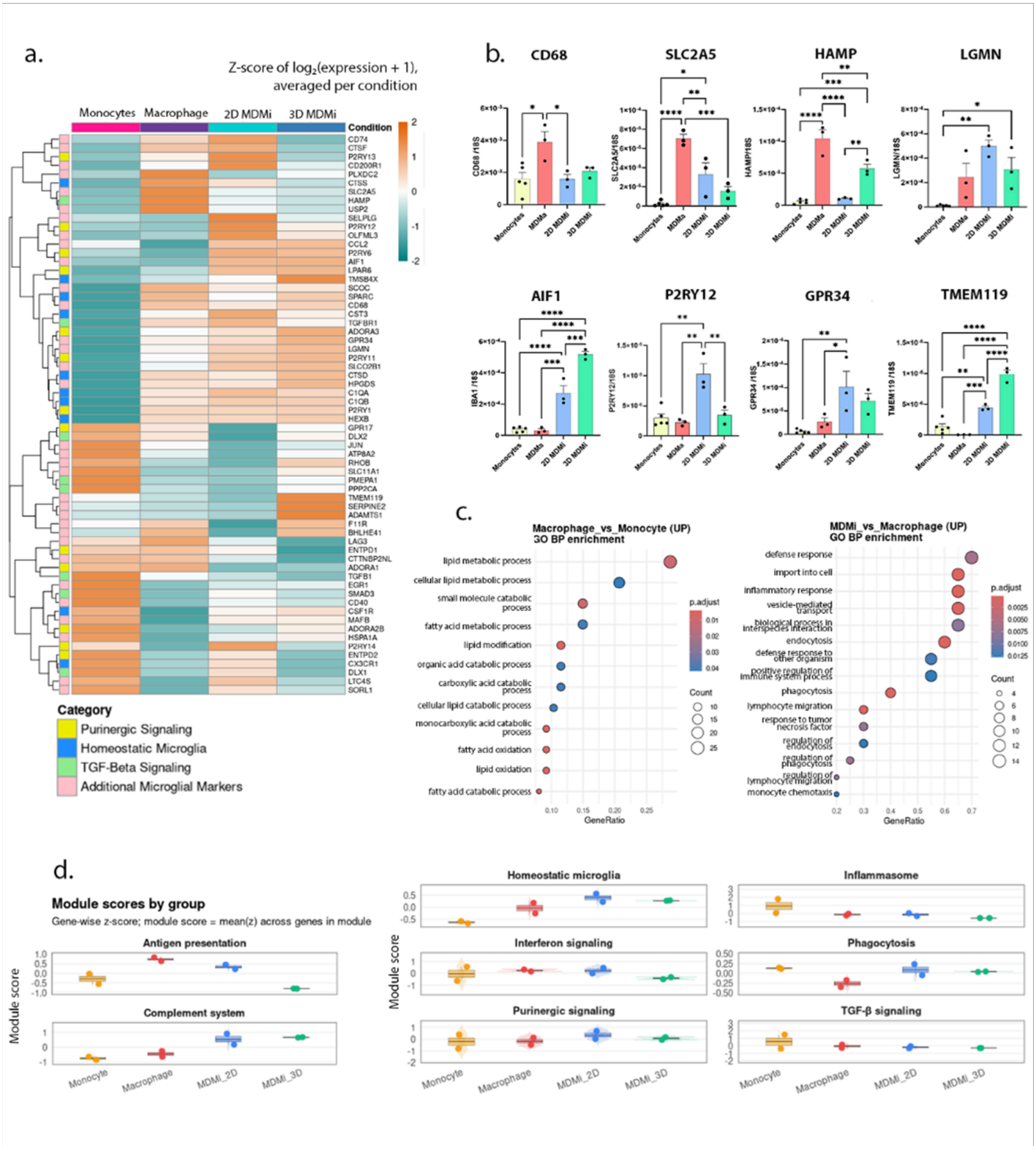


Figure 4

Transcriptional characterisation of monocytes, macrophages, 2D MDMi and 3D MDMi. (a) Heatmap of curated NanoString Glial Profiling Panel gene sets grouped into four categories: Purinergic Signalling, Homeostatic Microglia, TGF-β Signalling and Additional Microglial Markers. Values represent *z*-scores of log2-transformed expression averaged per condition. **(b)** Targeted qRT–PCR validation of selected macrophage- and microglia-associated genes across conditions. Data are shown as mean ± SD. $P < 0.05$ (*), $P < 0.01$ (**), $P < 0.001$ (***), $P < 0.0001$ (****). **(c)** GO biological process enrichment analysis comparing MDMa and MDMi states. **(d)**Module-score analysis summarising coordinated pathway activity across conditions. For each sample, module scores were calculated as the mean *z*-scored expression of genes within each module. Scores are shown as boxplots with individual sample values overlaid.

Supplementary Files

This is a list of supplementary files associated with this preprint. Click to download.

- SupplementaryFigureS3phagocytosisupdated.tif
- SupplementaryFigureS2QCfornanostringsamplescopy.tif
- SupplementaryFigureS1glialpanel.tif
- SupplementaryTable5Functionalmodulecomparisonacrossmicroglialmodels.xlsx
- SupplementaryTable4humanqpcrprimers.xlsx
- SupplementaryTable3DifferentiallyExpressedGenes.xlsx
- SupplementaryTable1Geneliststhemesannotations.xlsx
- SupplementaryTable2CountsNormalizedExpression.csv